Available online at www.sciencedirect.com
SCIENCE DIRECT®
Coordination Chemistry Reviews 249 (2005) 1902–1916
COORDINATION CHEMISTRY REVIEWS
www.elsevier.com/locate/ccr

Molecular mixed-valence cyanide bridged Co^{III}–Fe^{II} complexes

Paul V. Bernhardt [a,**], Fernando Bozoglián [b], Brendan P. Macpherson [a], Manuel Martínez [b,*]

[a] *Department of Chemistry, University of Queensland, Brisbane 4072, Australia*
[b] *Departament de Química Inorgànica, Universitat de Barcelona, Martí i Franquès 1-11, E-08028 Barcelona, Spain*

Received 8 September 2004; accepted 23 November 2004
Available online 5 January 2005

Contents

Abstract

Cyano-bridged mixed-valence compounds have been known for a long time, i.e., Prussian Blue polymeric solids. Nevertheless, the interest in discrete complexes having a well-defined molecular nuclearity has emerged more recently. There are numerous examples of cyano-bridged mixed-valence complexes in the recent literature, as they show promising and useful applications in electrochromism, molecular magnetism and molecular electronics. In this paper, the reactivity, synthetic and structural chemistry, as well as some physical and chemical properties, of a series of discrete dinuclear mixed-valence cyano-bridged complexes of general formulae $[L_nCo^{III}(\mu NC)Fe^{II}(CN)_5]^-$ (L = pentadentate macrocyclic ligand) are reviewed. Special emphasis is given to the synthetic strategy, redox properties and metal-to-metal-charge-transfer (MMCT) band energy. Tuning the MMCT transition energy has been possible by changing the redox potential of the metal centers, both through structural and outer-sphere changes. The redox processes that involve the appearance and disappearance of these MMCT bands in the visible region have been dealt with in relation to the possible uses of the complexes.

Keywords: Mixed-valence compounds; Metal-to-metal-charge-transfer band energy; Outer-sphere oxidation

1. Introduction

There is an increasing interest in cyano-bridged dinuclear mixed-valence complexes. This is, at least in part, due to their particular structural, redox, spectroscopic, and charge

* Corresponding author. Tel.: +34 93 4021273; fax: +34 93 4907725.
** Co-corresponding author. Fax: +61 7 3654299.
E-mail addresses: p.bernhardt@uq.edu.au (P.V. Bernhardt), manel.martinez@qi.ub.es (M. Martínez).

0010-8545/$ – see front matter © 2004 Elsevier B.V. All rights reserved.
doi:10.1016/j.ccr.2004.11.014

transfer properties. These make them potentially suitable for molecular electronics, e.g., electrochromic devices, solar energy conversion, magnetism, etc. [1,2].

Molecules bearing both oxidizing and reducing moieties have the possibility of displaying intramolecular electron transfer, as well as providing model complexes for the study of inner-sphere electron transfer processes [3–7]. Mixed-valence complexes, an example of these types of systems, played an important role in the development of the theory of electron transfer. *Mixed-valence* complexes contain two or more metal atoms in different formal oxidation states; *mixed oxidation-state* compounds would be a more accurate term, but they are designated *mixed-valence* for historical reasons. Two articles published in 1967 are key milestones in the development of this field.

Robin and Day surveyed a large number of mixed-valence compounds reported in the literature from as early as 1704, and including many naturally occurring mineral forms [8]. These were assigned into three broad categories according to the extent of delocalization between the mixed-valence centers, as determined from their electronic spectra, geometry and magnetochemistry. In *Class I* compounds, the redox active centers exhibit no coupling between them and hence may be treated as isolated independent metal centers. Only the properties of the individual metal complexes are observed. *Class II* compounds display a moderate degree of coupling between metal centers, which still display characteristics of distinct integral formal oxidation states (although slightly perturbed), but new properties arise due to the possibility of thermal and optical electron transfer between the redox centers. The theoretical framework concerning this class of compounds is discussed below. The compounds in *Class III* experience strong coupling between the metal centers, such that their oxidation states may no longer be considered as different integral values, but an average of the oxidation states involved. The electronic spectra of these compounds do not exhibit the properties of the component metal centers, but new spectral properties are instead observed. Contrarily to *Class II* complexes, currently no general comprehensive theoretical framework exists that describes the properties of *Class III* compounds.

The second piece of work developing the field was a two-part contribution by Hush. In the first paper along with Allen, a qualitative survey of solution and solid-state compounds displaying metal-to-metal-charge-transfer (MMCT), or intervalence charge transfer (IVCT), absorption was conducted [6]. The second part set out the theory relating spectroscopic data to thermodynamic parameters [4]. The appeal of Hush's work was that it provided a means by which the optical MMCT transition could be correlated with the energetic barrier to thermally activated electron transfer. Moreover, analysis of spectral band shapes provides information on reorganizational parameters, coupling between metal centers and the degree of electron delocalization. The same practical approach as that establishing the validity of outer-sphere redox mechanisms according to Marcus theory has been applied [9]. That is, agreement of an experimental bandwidth with that calculated from Hush theory has been taken as a test for whether or not a compound can be considered as falling within the Robin and Day's *Class II* category.

In this system of weakly interacting metal centers, *Class II*, thermal electron transfer from one site to the other is always possible whenever a radiative transition is observed. Hush's work provides a means of correlating these two forms of electron transfer. In a symmetric mixed-valence complex, the reactant and product of the electron transfer process have the same free energy. Based on the assumption that the potential energy surfaces are parabolas of the same curvature, the energy of the MMCT transition E_{op} is, by algebraic reasons, four times the energy barrier to thermal electron transfer $\Delta G^{\ddagger}$ (Eq. (1)).

$$E_{op} = 4\,\Delta G^{\ddagger} \tag{1}$$

Even though the initial and final states of the MMCT reaction are the same, the structure of the complex and the solvent interactions change as a result of the shift in charge density. According to the Franck–Condon principle, this reorganization is much slower than the electron transfer step and energy is needed to promote electron transfer. This amount of energy is known as the reorganization energy, λ, and is equal to the energy of the MMCT transition (Eq. (2)) for symmetric complexes.

$$E_{op} = \lambda \tag{2}$$

Hush and Creutz viewed the energy difference between the excited and ground state redox isomers as an internal energy term ΔE [4,5]. Marcus has argued that it is better viewed as a free energy term, ΔG°, since according to the Franck–Condon principle there is no change in the momenta or coordinates of the nuclei immediately before and after the transition, and hence there is no entropy change associated with the transition [7,10]. While temperature dependent experiments carried out by Hupp et al. seem to support the free energy approach [10], the issue remains unresolved [11]. The free energy terminology is used here (ΔG° and λ, cf. ΔE and χ in Hush's work).

In the case of asymmetric complexes, the reactant and product states no longer have the same energy (Fig. 1). The energy of the MMCT transition in this case is equal to the energy difference between the initial and final states, plus the reorganizational energy (Eq. (3)).

$$E_{op} = \Delta G^{\circ} + \lambda \tag{3}$$

ΔG° can be estimated from the difference between the redox potentials of the donor and acceptor metal centers, since charge transfer effectively involves simultaneous oxidation of the donor and reduction of the acceptor. This assumes that the redox potential of one metal center is not affected in an important way by the oxidation state of the adjacent metal center, or that such effects for the donor and acceptor cancel out.

As for the reorganization energy, it involves inner- (λ_i) and outer-sphere (λ_o) contributions. The inner-sphere contribution results from bond length and conformational changes, and can be estimated from a summation of these changes over each of the metal–ligand bonds in the initial and final states by treating the centers as classical harmonic oscillators [7,11]. The outer-sphere contribution, arising from changes in the solvent orientation following internal electron transfer, may be calculated in a number of different ways, depending on the model chosen (the simplest being that of non-penetrating spheres within a dielectric continuum). The simpler models break down when specific solvent–solute effects are active, such as H-bonding between the complex and the solvent. In complexes bearing am(m)ine and cyano ligands, specific solvent interactions are significant [11]. In this case, the empirical donor number (DN) and acceptor number (AN) terminology is commonly invoked to explain such effects [12].

The energetic scheme depicted in Fig. 1 produces an important relationship between thermodynamic and kinetic parameters related to the internal electron transfer process (Eq. (4)) [7].

$$\Delta G^{\neq} = \frac{E_{op}^2}{4\lambda} = \frac{(\lambda + \Delta G^{\circ})^2}{4\lambda} \quad (4)$$

The equation allows for the determination of dynamic ($\Delta G^{\neq}$) thermal parameters for the electron transfer processes from the knowledge of static and thermodynamic measures (E_{op} and ΔG°). This approximation has been used frequently to good effect [13,14], revealing important specific solvent–solute interactions affecting the electron transfer process [15,16].

It is important to note that the relationships developed by Hush are applicable only in the high-temperature limit; they are fundamentally classical in the way that both the inner-shell and solvent are treated. Other theoretical treatments have been put forth, which take quantum effects in the inner-shell into account. In particular the model developed by Piepho et al., which treats only symmetric inner-shell vibronic modes and neglects the effect of the solvent shell, has gained the greatest attention [17]. Given that the MMCT transitions of many complexes exhibit solvatochromic shifts, this omission is a major drawback of the model.

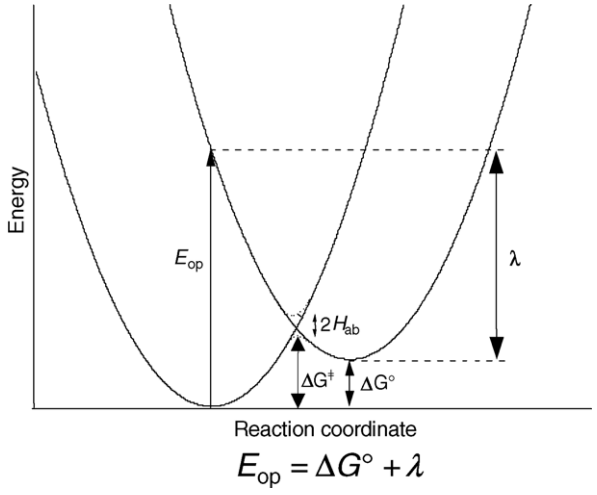

Fig. 1. Potential energy surface of an asymmetric mixed-valence complex.

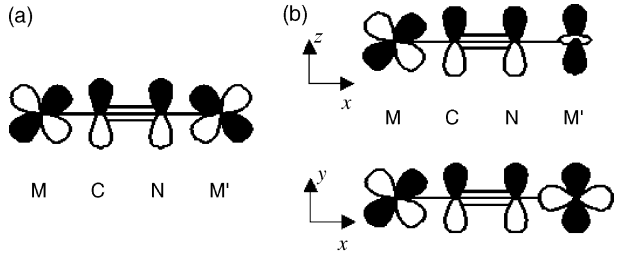

Fig. 2. Orbital overlap of (a) some t_{2g}–t_{2g}' orbitals, and (b) t_{2g}–e_g orbitals for a cyanide bridged compound.

MMCT transitions involving pseudo-octahedrally coordinated d-block ions are subjected to the usual symmetry requirements (Fig. 2).

Thus, from filled t_{2g} orbitals of the donor the possibility of intervalence transfer into either t_{2g}' or e_g' unfilled acceptor orbitals exists in many cases [3]. In Prussian blue (ferric ferrocyanide, a low spin d^5–d^6, cyano-bridged coordination polymer) the two transitions have been observed and they differ by ca. 10,000 cm^{-1}, which corresponds to ΔO_h in the Fe^{III} acceptor [3,18,19]. The symmetry requirements depicted in Fig. 2 explain why the lower energy for the transition between the t_{2g} orbitals has a greater intensity than that between the orthogonal t_{2g} and e_g' orbitals. The values of the extinction coefficients for the systems indicated in Table 1 agree very well with this simple qualitative approach; [3,4,18,19] the lower ε corresponding to systems with acceptor t_{2g}' orbitals completely filled.

Of course, the symmetry of the system is not O_h in these dinuclear complexes, and the three ideally degenerate t_{2g} orbitals, are split by both effects due to low symmetry ligand fields and to spin–orbit coupling [20,21]. As a consequence the MMCT band may be broadened, since it can actually be made up of three closely overlapping bands due to transitions originating from three different t_{2g} orbitals. If spin–orbit coupling is large, as it is for second and third transition series, separate bands corresponding to each of the spin–orbit coupled states may be resolved (as observed in cyano-bridged osmium complexes) [20,22]. Furthermore, the lowest energy d_π orbitals with components in the direction of the bridge will produce more intense symmetry-allowed transitions, inducing a shift to higher energy for the final convoluted signal.

Electronic coupling between metal centers occurs through the bridging ligand orbitals. The bridging group has a structural role in keeping the metal centers at a fixed distance apart and an electronic role in providing communication between the metal centers [41]. Many nitrogen-substituted aromatic heterocycles have been used as bridging ligands between ruthenium centers [5] since the now famous, symmetrical

Table 1
Survey of cyano-bridged dinuclear complexes

Species	MMCT, λ (cm^{-1})	ε ($M^{-1}\,cm^{-1}$)	Reference
$[(NC)_5Co(\mu\text{-}NC)Fe(CN)_5]^{6-}$	26000	630	[23,24]
$[(H_3N)_5Co(\mu\text{-}NC)Co(CN)_5]$	–	–	[25]
$[(H_3N)_5Co(\mu\text{-}CN)Co(CN)_5]$	–	–	[26]
$[(H_3N)_5Ru(\mu\text{-}NC)Fe(CN)_5]^{-}$	10200	3000	[27]
$[(H_3N)_5Co(\mu\text{-}NC)Ru(CN)_5]^{-}$	26670	690	[28]
$[(NC)_5Co(\mu\text{-}NC)Ru(CN)_5]^{6-}$	32050	460	[24]
$[(NC)_5Co(\mu\text{-}NC)Os(CN)_5]^{6-}$	27780	734	[29,30]
$[(H_3N)_4(H_2O)Cr(\mu\text{-}NC)Fe(CN)_5]^{-}$	26595	2500	[29]
$[(H_3N)_5Ru(\mu\text{-}NC)Os(CN)_5]^{-}$	12050	3450	[31]
$[(H_3N)_5Ru(\mu\text{-}NC)Ru(CN)_5]^{-}$	14700	2800	[32]
$[(NC)_5Fe(\mu\text{-}NC)Fe(CN)_5]^{6-}$	7690	ca. 10^3	[33]
$[(H_3N)_5Os(\mu\text{-}NC)Fe(CN)_5]^{-}$	15920	1640	[30]
$[(H_3N)_5Os(\mu\text{-}NC)Ru(CN)_5]^{-}$	20400	1840	[30]
$[(H_3N)_5Os(\mu\text{-}NC)Os(CN)_5]^{-}$	17890	2090	[30]
$[(EDTA)Ru(\mu\text{-}NC)Fe(CN)_5]^{5-}$	10640	2700	[34,35]
$[(EDTA)Ru(\mu\text{-}NC)Ru(CN)_5]^{5-}$	14840	2800	[35]
$[(EDTA)Ru(\mu\text{-}NC)Os(CN)_5]^{5-}$	13120	2900	[35]
$[(H_3N)_5Cr(\mu\text{-}NC)Fe(CN)_5]^{-}$	26670	2400	[30,36]
$[(NC)_5Ru(\mu\text{-}NC)Fe(CN)_5]^{6-}$	12420	–	[37]
$[(H_3N)_5Pt(\mu\text{-}NC)Fe(CN)_5]$	23750	540	[38]
$[(EDTA)Co(\mu\text{-}NC)Fe(CN)_5]^{5-}$	ca. 17860[a]	–	[39,40]

[a] Obtained as unstable intermediate.

Creutz–Taube ion $[(H_3N)_5Ru(\mu\text{-pyrazine})Ru(NH_3)_5]^{5+}$ was first synthesized [42]. These compounds range in their degree of coupling from weak to strong, and hence cover the Robin and Day's, *Classes II* and *III* categories. The MMCT transitions of symmetric mixed-valence complexes usually fall within the near-infrared region of the spectrum.

Cyanide is another suitable bridging ligand that allows moderate coupling between the metal centers it spans. The cyano-ligand is an ambidentate ligand bearing donors with quite distinct binding properties [41,43]. Although polymeric materials such as Prussian blue and analogous materials containing different metal centers have long been known, discrete cyano-bridged complexes with well-defined structures and nuclearity are less common, but are important in enabling the many facets of MMCT transitions to be delineated [41]. Another advantage of studies involving cyano complexes in particular is that metal-to-ligand-charge transfer bands usually occur at high energies (UV region), and hence do not overlap with MMCT bands in the NIR-visible region [44].

The first dinuclear cyano-bridged complex, $[(NC)_5Co(\mu\text{-}NC)Fe(CN)_5]^{6-}$), was isolated in 1961 [23], as a product of an inner-sphere electron transfer reaction between $[Co(CN)_5]^{3-}$ with $[Fe(CN)_6]^{3-}$. The complex exhibits an MMCT transition at 385 nm. The preparation of two linkage isomers $[(H_3N)_5Co(\mu\text{-}NC)Co(CN)_5]$ and $[(H_3N)_5Co(\mu\text{-}CN)Co(CN)_5]$ has also been reported; [25,26] the bridging mode being assigned on the basis of the electronic spectra of the complexes. The preparation and the kinetics of formation of the complex $[(H_3N)_5Ru(\mu\text{-}NC)Fe(CN)_5]^{-}$, which exhibits an MMCT transition at 980 nm, has also been studied [27].

A thorough investigation of photochemical reactions of dinuclear cyano-bridged mixed-valence complexes induced by excitation into the MMCT band has been conducted [24,28–30,45,46]. In particular, the reactions involving pentacyanocobaltate(III) and pentamminecobalt(III) bridged to hexacyanometallates (Fe, Ru, Os) have been studied; irradiation of $[(H_3N)_5Co(\mu\text{-}NC)Ru(CN)_5]^{-}$ into its MMCT bands results in decomposition of the complex. The photochemical reaction only takes place if the rate of reaction is able to compete with the back-electron transfer reaction. Attempts to prepare the iron analogue $[(H_3N)_5Co(\mu\text{-}NC)Fe(CN)_5]^{-}$ failed, apparently due to the lower redox potential of $[Fe(CN)_6]^{4-}$ with respect to $[Ru(CN)_6]^{4-}$, resulting in reduction of the cobalt center followed by dissociation of the labile Co^{II} ammine intermediate [29]. We shall return to this point later in the discussion of the synthetic strategies that become possible when monodentate ammine ligands are replaced multidentate macrocyclic amines.

The dinuclear iron complex $[(NC)_5Fe(\mu\text{-}NC)Fe(CN)_5]^{6-}$ has been prepared by equimolar reaction of $[Fe(CN)_5(NH_3)]^{2-}$ with $[Fe(CN)_6]^{4-}$ and purification using ion exchange chromatography [33]. Spectroelectrochemical experiments revealed that the MMCT transition, observed at 1300 nm, is lost upon oxidation or reduction to the Fe^{III}–Fe^{III} and Fe^{II}–Fe^{II} forms, respectively. The mixed-valence Fe^{III}–Fe^{II} form exists at poised potentials between ca. 100 and 300 mV (versus SCE). This fact opens up the possibility of studying the chemical and electrochemical redox processes of these compounds, as will be treated later in the review.

The complex $[(EDTA)Ru(\mu\text{-}NC)Fe(CN)_5]^{5-}$ has been synthesized and its redox kinetics studied as well as the temperature dependence of the MMCT band [34,47]. The temperature dependence of the MMCT bands and $Ru^{III/II}$ and $Fe^{III/II}$ redox potentials of the related $[(H_3N)_5Ru(\mu\text{-}NC)Fe(CN)_5]^{-}$

have also been studied [34,48]. A good correlation between the temperature-induced shifts in MMCT transition energy and redox couple difference (ΔE°) has been determined.

The series of Ru/EDTA complexes has been extended to Ru and Os cyanides [21]. The equilibria of formation for dinuclear and trinuclear ([(EDTA)Ru(μ-NC)M(CN)$_4$(μ-CN)Ru(EDTA)]$^{6-}$) complexes has been examined in great detail. A μ-cyano Co/EDTA dinuclear complex has been found to form as an intermediate in the reaction of [Co(EDTA)]$^{2-}$ and [Fe(CN)$_6$]$^{3-}$, which decomposes to [Co(EDTA)]$^{-}$ and [Fe(CN)$_6$]$^{4-}$ [49].

A related pair of di- and tri-nuclear mixed-valence complexes has also been investigated [38,50]. The trinuclear low spin Fe^{II}–Pt^{IV}–Fe^{II} complex [(NC)$_5$Fe(μ-CN)Pt(NH$_3$)$_4$(μ-NC)Fe(CN)$_5$]$^{4-}$ may undergo intervalence transfer from each ferrocyanide donor to form (square planar) Pt^{II}, which results in dissociation upon prolonged irradiation. This effect has been utilized for photochemical formation of patterned Prussian blue surfaces on ITO glass, by irradiating the complex in a Fe(NH$_3$)$_4$(SO$_4$) solution [51]. Prussian blue is formed from the reaction of [Fe(CN)$_6$]$^{3-}$, produced by photodegradation of the complex, with Fe^{2+}. Both the trinuclear and dinuclear ([(H$_3$N)$_5$Pt(μ-NC)Fe(CN)$_5$]) complexes have been structurally characterized.

It is clear that the efficiency of optical or thermal electron transfer is determined in an important manner by the redox parameters of the metal centers. These redox characteristics are dependent on the nature of the ligands and their environment, including interactions within the first solvation sphere. In principle, the redox, optical and kinetic properties of mixed-valence compounds can be tuned by choosing the appropriate ligand and solution medium [52]. This requires systematic studies of the abovementioned factors. However, discrimination between these contributions and their effect on the redox properties of metal redox centers from a quantitative point of view is a complicated task. One of the inherent problems of cyano-bridged Co^{III} complexes is that the acceptor, upon reduction, either electrochemically or through MMCT excitation, is rendered labile (Co^{II}) and is susceptible to facile ligand dissociation. In an effort to stabilize the complex against electrochemical or photochemical degradation, we have utilized pentadentate macrocyclic amine and mixed donor ligands coordinated to the Co^{III} center. It will be compounds of this type ([L$_n$Co(μ-NC)Fe(CN)]$^{-}$; L$_n$ being a pentadentate, amino-appended *n*-membered macrocyclic tetraamine or diamine dithioether) that will be the focus of this review.

2. Preparative strategy

The preparation of the mixed-valence complexes, *cis*/*trans*-[L$_n$Co^{III}(μ-NC)Fe^{II}(CN)$_5$]$^{-}$, can be easily achieved via a substitution process of a relatively labile ligand on an inert Co^{III} center by the {Fe^{II}(CN)(L)$_5$} species to produce the corresponding μ-cyano Co^{III}–Fe^{II} complex, where the C-atom of the bridging ligand remains coordinated to Fe (Scheme 1).

Typically, long reaction times are required when ligand substitution is attempted on the inherently inert Co^{III} center. However, we have developed a preparative strategy for these dinuclear complexes that takes advantage of the mechanisms operating for redox and substitution processes of Co$^{III/II}$ and Fe$^{II/III}$ metal centers [53,54]. The overall process had already been established for Co^{III}/EDTA systems some time ago [40,55,56], but the use of carefully controlled conditions derived from the mechanistic knowledge of outer-sphere reduction and substitution processes on [CoL$_n$(H$_2$O)]$^{3+}$ enabled us to fully characterize the complexes [53,54,57–59]. The method takes advantage of the inertness of amino Co^{III} and cyano Fe^{II} complexes (that in combination undergo redox reactions) and the labile character of the reduced amino Co^{II} complex formed while the oxidized Fe^{III} cyano complex retains its inertness (Scheme 2) [60,61].

Alternatively, direct aqua ligand substitution on the Co^{III} center by [Fe^{III}(CN)(L)$_5$]$^{3-}$ can also be achieved by using longer reactions times producing the oxidized [L$_n$Co^{III}(μ-NC)Fe^{III}(CN)$_5$] form of the complexes. The intrinsic inertness of the Co^{III} ion can be circumvented by carrying out the substitution reaction at alkaline pH. Under these conditions, a base-assisted substitution mechanism applies for these Co^{III} complexes and the reactions are accelerated considerably [62]. The final complex in these reactions is, surprisingly, the reduced mixed-valence [L$_n$Co^{III}(μ-NC)Fe^{II}(CN)$_5$]$^{-}$ form. This indicates that under these conditions a subsequent reduction reaction occurs, as will be indicated later when reviewing the redox processes involving these complexes.

The use of these mechanistically inspired preparative processes has been successful for the systems derived from the Co^{III} moieties indicated in Scheme 3.

All of these compounds have been characterized and the reproducibility of the preparative processes established [63–67]. Changes in isomerism from *cis*-L$_{14}$ to *trans*-L$_{14}$, *cis*-L$_{14S}$ to *trans*-L$_{14S}$ and *cis*-L$_{15}$ to *trans*-L$_{15}$ upon dinuclear preparation have been noted [65]. Further studies on

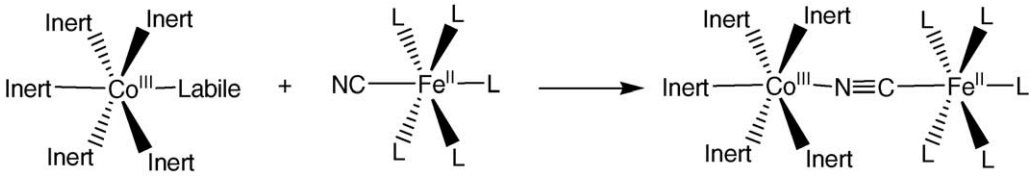

Scheme 1.

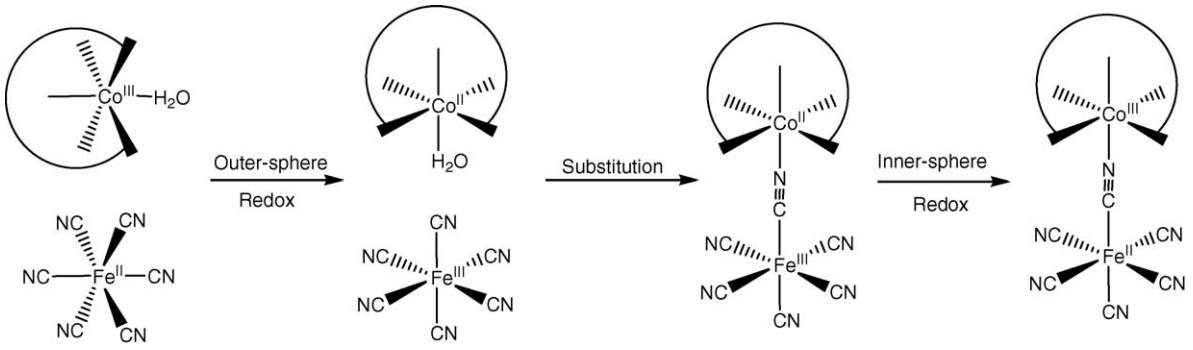

Scheme 2.

the precursor Co^{III} complexes, *cis*-L_{14} and *cis*-L_{15}, indicated that these compounds isomerize to their *trans* derivatives on a similar workup to that employed for the dinuclear complexes [68]. This fact agrees with the inherent stabilities of the cobalt and iron skeleton upon mixed-valence Co^{III}–Fe^{II} complex formation. The crystal structures of the dinuclear cyano-bridged Co^{III}–Fe^{II} complexes bearing the macrocycles *cis*-L_{14}, *trans*-L_{14}, *trans*-L_{15} and *trans*-L_{14S} have been determined as well as those corresponding to the oxidized Co^{III}–Fe^{III} forms of the same complexes.

Electrochemistry of the dinuclear Co^{III}–Fe^{II} complexes indicates that, although they are weaker reductants (by ca. 200 mV) than ferrocyanide, they are still able to participate in outer-sphere electron transfer reactions with mononuclear Co^{III} precursors. This fact enables us to further apply the preparative scheme indicated above using $[L_nCo^{III}(\mu\text{-}NC)Fe^{II}(CN)]^-$ as the reducing agent of the mononuclear Co^{III} amine complex. An example of this possible building block strategy is indicated in Scheme 4.

These studies are currently underway and open up the possibility of further increasing the nuclearity of the complexes. In compounds of the type $[L_nCo(\mu\text{-}NC)Fe(CN)_4(\mu\text{-}CN)CoL_n]^{2+}$, the charge of the complex is the same as that of the mononuclear Co^{III} reductant, and the $Fe^{III/II}$ is raised by an additional 200 mV due to the influence of the second $\{L_nCo^{III}\}$ moiety, so the formation of higher nuclearity species will be unfavourble. This is a very useful feature as it may facilitate the possible preparation of unsymmetrical complexes as these indicated in Scheme 5.

3. Factors affecting the MMCT energy

As already indicated, and according to Hush theory for asymmetric *Class II* mixed-valence complexes (Eq. (3)), the MMCT transition energy (E_{op}) is the sum of the free energy difference between the two redox isomers ΔG°, e.g., Co^{III}–Fe^{II} and Co^{II}–Fe^{III}, and the reorganizational energy

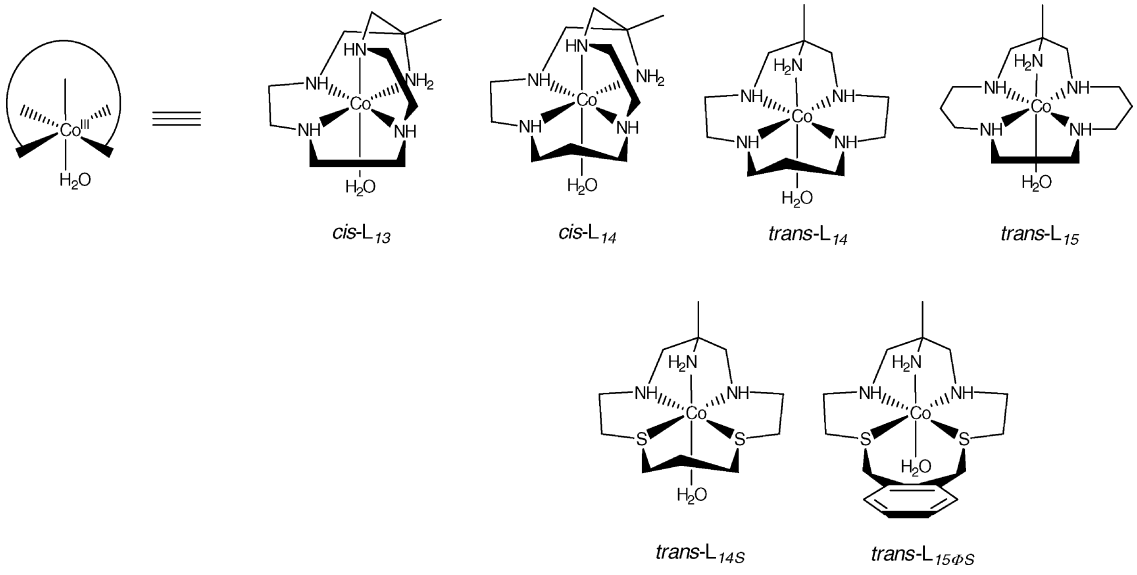

Scheme 3.

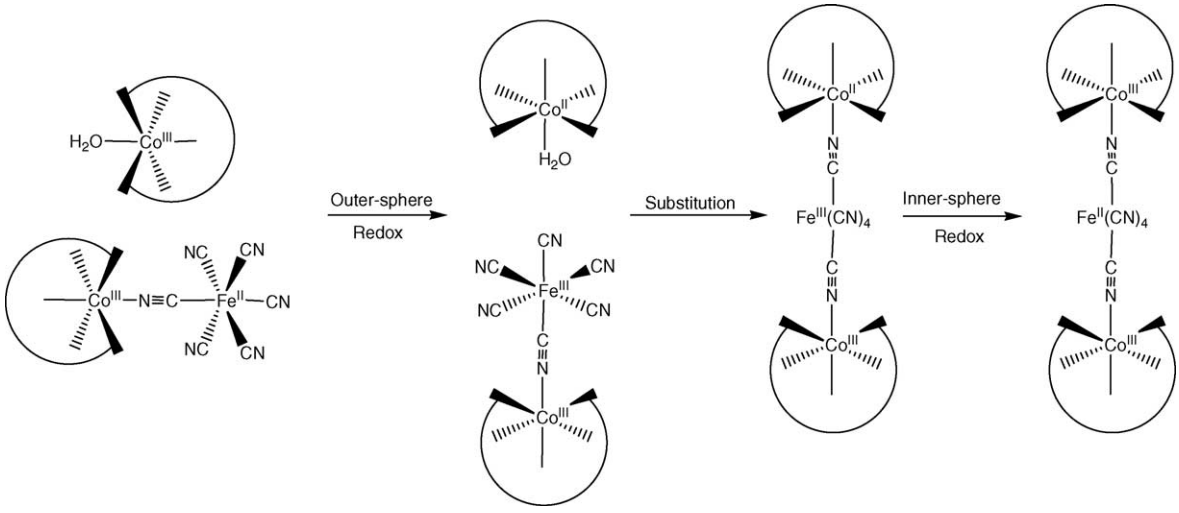

Scheme 4.

(λ), which is a sum of both inner- and outer-sphere processes. In principle, all three terms in Eq. (3) may be measured independently: the MMCT energy E_{op} (cm^{-1}); redox potential difference (ΔG° (cm^{-1}) = $\Delta E^{\circ}F/11.97$) and the MMCT bandwidth at half height (at $300K$, λ (cm^{-1}) = $(\Delta\bar{\nu}_{1/2})^2/2310$). Of these three experimental values, the bandwidth at half height ($\Delta\bar{\nu}_{1/2}$) is the most prone to error. An accurate measurement of $\Delta\bar{\nu}_{1/2}$ is crucial given the fact that for a Gaussian-shaped band λ is proportional to the square of the bandwidth, i.e., error propagation will be large if a poor estimate of $\Delta\bar{\nu}_{1/2}$ is made. In all of the spectra, we shall discuss from compounds that we have made, the MMCT transition overlaps with d–d bands from the Co^{III} chromophore so an accurate measurement of $\Delta\bar{\nu}_{1/2}$ is not possible. Spectral deconvolution techniques may be applied assuming Gaussian band shapes. However, this introduces a potentially major systematic error if more than one combination of bands matches the experimental spectrum. A further complication arises from spin–orbit coupling in the excited state [20], which may split the MMCT transition; leading to band asymmetry and broadening depending on the magnitude of the coupling constant. This is most significant in second and third row transition elements. For this reason, we have chosen to use Eq. (3) to calculate λ using accurately determined values of E_{op} and ΔG°.

As the dinuclear compounds discussed herein comprise a homologous series (same charge, structurally similar ligands, low spin d^6–d^6 electronic configurations, etc.) variations in the reorganizational energy (λ) should not be very large. It then emerges that only significant variables in determining the MMCT energy are the redox potentials of the donor and acceptor.

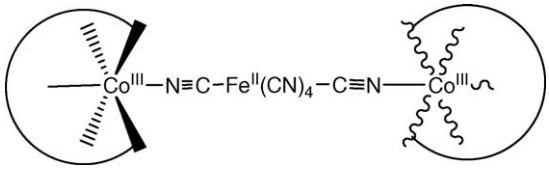

Scheme 5.

Taking the compound *trans*-$[L_{14}Co^{III}(\mu\text{-}NC)Fe^{II}(CN)_5]^-$ as a benchmark, there are four structural variables that we have changed (one at a time) so as to alter the redox isomer free energy difference, and thus tune the MMCT transition energy in a rational way. These are the following:

- macrocyclic ring size (acceptor);
- geometric isomeric form (acceptor);
- macrocyclic donor atoms (acceptor);
- cyanometallate unit (donor).

3.1. Macrocyclic ring size

Since the early days of synthetic macrocyclic chemistry (e.g., the crown ethers), it has been well known that macrocycles of various sizes will form more stable complexes with metal ions where there is a match between the ionic/covalent radius of the metal and the preferred 'hole' size of the ligand. A mismatch between the preferences of the metal and ligand will lead to internal strain manifested in bond lengths, angles and dihedral angles deviating from their ideal values and non-bonded repulsion between atoms constrained to be in proximity. The result is decreased thermodynamic stability of the complex. The potential of a redox couple is dependent on many terms, but molecular mechanics calculations on a series of Co^{III} hexaamines [69] found that the calculated strain energy difference between the oxidized (Co^{III}) and reduced (Co^{II}) form of the couple was strongly correlated with the experimentally determined redox potential. As the ionic radius of the metal increases upon reduction, ligands that cannot cope readily with this expansion are subject to large strain energy differences upon reduction and consequently a very low potential $Co^{III/II}$ redox couple is found.

Table 2
Spectroscopic and electrochemical data (vs. NHE) for dinuclear complexes where the ring size, geometric isomerism and ligand donor atoms are varied

Species	E_{op} (cm^{-1})	E°_{red} [$Fe^{III/II}(CN)_6$] (mV)	E°_{red} ($Co^{III/II}$) (mV)	ΔG° (cm^{-1})[a]	λ (cm^{-1})[b]
trans-[L_{14}Co(μ-NC)Fe$(CN)_5$]$^-$	19600	630	−600	9800	9800
trans-[L_{15}Co(μ-NC)Fe$(CN)_5$]$^-$	18400	600	−580	9400	9000
cis-[L_{14}Co(μ-NC)Fe$(CN)_5$]$^-$	19600	600	−500	8800	10800
trans-[L_{14S}Co(μ-NC)Fe$(CN)_5$]$^-$	17500	640	−350	7900	9600

[a] Calculated from $\Delta E^{\circ}F/11.97$.
[b] Calculated from Eq. (3).

We have fully characterized the pair of complexes *trans*-[$L_{14}Co^{III}$(μ-NC)$Fe^{II}(CN)_5$]$^-$ [64] and *trans*-[$L_{15}Co^{III}$(μ-NC)$Fe^{II}(CN)_5$]$^-$ [43] where the only difference is the ring size of the macrocyclic ligands. The relevant spectroscopic and electrochemical data are summarized in Table 2. It is apparent that the MMCT energies (Fig. 3, indicated by arrows) are very similar. Furthermore, the respective electrochemically determined $Fe^{III/II}$ and $Co^{III/II}$ redox potentials are essentially the same, which implies that differences between the two reorganizational energies are small.

3.2. Geometric isomeric form

Like its parent ligand cyclam, the macrocyclic secondary amines of L_{14} may coordinate in either a coplanar (*trans*) or folded (*cis*) configuration and we have isolated both forms of their respective dinuclear complexes *trans*-[L_{14}Co(μ-NC)Fe$(CN)_5$]$^-$ and *cis*-[L_{14}Co(μ-NC)Fe$(CN)_5$]$^-$ [65]. The electronic spectra of the isomers are shown in Fig. 4 and the spectroscopic data appear in Table 2.

This isomeric pair of complexes illustrates an interesting and subtle feature where the redox isomer free energy change and the reorganizational energies each change going from one isomer to the other, but in opposite directions; resulting in no significant change to the MMCT energy. Indeed the two effects may be (inversely) correlated. Firstly, the $Co^{III/II}$ redox potential for the *cis* isomer is ca. 100 mV more positive than the *trans* isomer. All other things being equal in this special isomeric pair, it emerges that the greater ease of reduction seen for the *cis* isomer points to less strain being introduced to the complex upon reduction. Molecular mechanics calculations [65] supported this hypothesis where the folded macrocycle is better able to cope with the Co–N bond expansion upon reduction. However, the calculations also predict that the Co–N bond lengths in the *cis* isomer increase by a greater amount upon reduction than the *trans* isomer, which encircles the metal ion and opposes substantial changes to its Co–N bond lengths. The point is that the greater Co–N bond length extension in the *cis* isomer should result in a greater value of the inner-sphere reorganizational energy and hence the overall reorganizational energy λ, as observed (Table 2). Outer-sphere redox processes of *cis*-[$CoL_{14}(H_2O)]^{3+}$ and *trans*-[$CoL_{14}(H_2O)]^{3+}$ complexes show practically the same values of $\Delta G^{\neq}$ [54].

3.3. Macrocyclic donor atoms

More profound changes to the $Co^{III/II}$ redox potential may be achieved by replacing some of the N-donors by softer S-donors. Qualitatively one would expect an anodic shift in the $Co^{III/II}$ redox potential upon introduction of S-donors into the coordination sphere and this is in fact what we have observed [67].

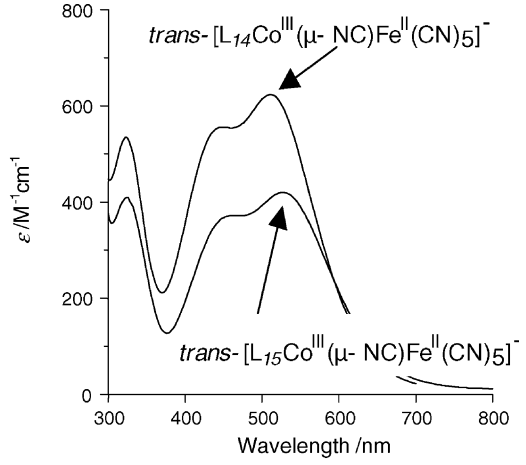

Fig. 3. Electronic spectra of *trans*-[$L_{14}Co^{III}$(μ-NC)$Fe^{II}(CN)_5$]$^-$ and *trans*-[$L_{15}Co^{III}$(μ-NC)$Fe^{II}(CN)_5$]$^-$.

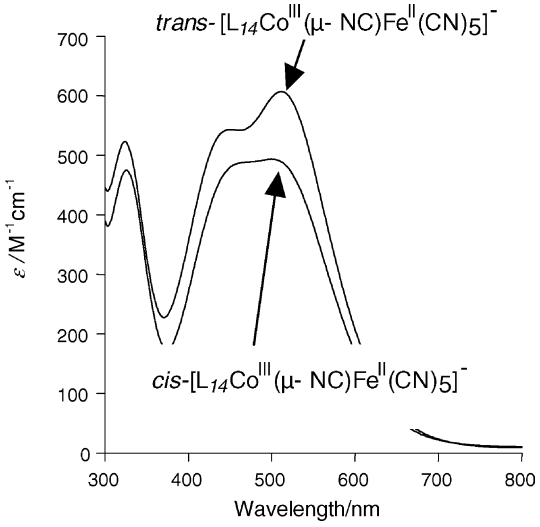

Fig. 4. Electronic spectra of *trans*-[$L_{14}Co^{III}$(μ-NC)$Fe^{II}(CN)_5$]$^-$ and *cis*-[$L_{14}Co^{III}$(μ-NC)$Fe^{II}(CN)_5$]$^-$.

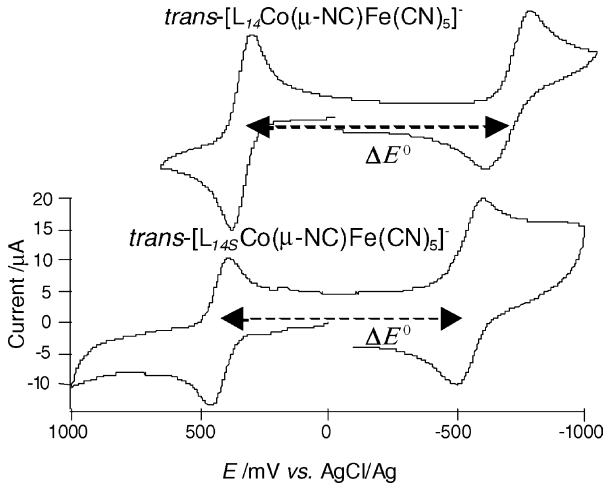

Fig. 5. Cyclic voltammograms (glassy carbon working electrode, 100 mV s^{-1}) of *trans*-$[L_{14}Co^{III}(\mu\text{-NC})Fe^{II}(CN)_5]^-$ (top) and *trans*-$[L_{14S}Co^{III}(\mu\text{-NC})Fe^{II}(CN)_5]^-$ (bottom).

The cyclic voltammograms of *trans*-$[L_{14}Co^{III}(\mu\text{-NC})Fe^{II}(CN)_5]^-$ and *trans*-$[L_{14S}Co^{III}(\mu\text{-NC})Fe^{II}(CN)_5]^-$ are shown in Fig. 5. The ca. 200 mV anodically shifted $Co^{III/II}$ couple for the thioether analogue leads to a significant decrease in the MMCT energy. The reorganizational energies are essentially unaffected, which is consistent with each complex bearing a 14-membered macrocyclic ligand in a *trans* coordination mode. The shift in the MMCT maximum to lower energy (Table 2) is evident from the colour of *trans*-$[L_{14S}Co^{III}(\mu\text{-NC})Fe^{II}(CN)_5]^-$ (purple) as distinct from *trans*-$[L_{14}Co^{III}(\mu\text{-NC})Fe^{II}(CN)_5]^-$, *cis*-$[L_{14}Co^{III}(\mu\text{-NC})Fe^{II}(CN)_5]^-$ and *trans*-$[L_{15}Co^{III}(\mu\text{-NC})Fe^{II}(CN)_5]^-$ (maroon-red).

3.4. Cyanometallate unit

The most significant differences in the MMCT energy are brought about by changes in the cyanometallate unit. Nitrile protonation of the $\{Fe^{II}(CN)_6\}$ moiety on the dinuclear complex brings in dramatic changes in the UV–vis spectra as indicated in Fig. 6.

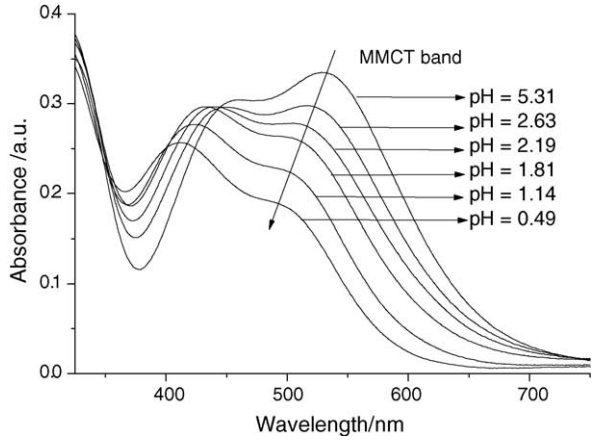

Fig. 6. UV–vis spectral changes obtained for a solution 1×10^{-3} M of complex *trans*-$[L_{15}Co^{III}NCFe^{II}(CN)_5]^-$ on changing the acidity conditions.

Table 3
Spectroscopic and electrochemical data (vs. NHE) for complexes $[L_nCo^{III}(\mu\text{-NC})Fe^{II}(CN)_3(CNH)_2]^+$

Species	E_{op} (cm^{-1})	E°_{red} ($Fe^{III/II}$) (mV)
trans-$[L_{14}Co(\mu\text{-NC})Fe(CN)_5(CNH)_2]^+$	20700	780
trans-$[L_{15}Co(\mu\text{-NC})Fe(CN)_5(CNH)_2]^+$	21200	770
trans-$[L_{14S}Co(\mu\text{-NC})Fe(CN)_5(CNH)_2]^+$	20400	800

The values determined for the protonation equilibrium indicated that two consecutive protonation steps occur ($p\beta_{12}$ ca. 2.1). Spectrophotometric and potentiometric titrations indicated that the monoprotonated complexes, $[L_nCo^{III}(\mu\text{-NC})Fe^{II}(CN)_4(CNH)]$, are never the sole species present in solution at any pH, and only the complexes $[L_nCo^{III}(\mu\text{-NC})Fe^{II}(CN)_3(CNH)_2]^+$ represent the composition of the solution at 1.0 M $HClO_4$ [66]. The UV–vis spectral and $Fe^{III/II}$ redox potential data of these doubly protonated complexes are collected in Table 3.

The correlation between the changes in the metal-to-metal-charge-transfer energy and the increase of the iron redox potential is very clear. The values indicate that, provided the redox potential on the cobalt center is unchanged from the deprotonated complexes, the increase of ca. 160 mV on the iron reduction potential on nitrile protonation (Fig. 7) translates very well in an increase of ca. 1500–2500 cm^{-1} in the energy corresponding to the MMCT band. Unfortunately, the conditions that are needed for the existence of the $[L_nCo(\mu\text{-NC})Fe(CN)_5(CNH)_2]^+$ complexes ($[H^+] = 1.0$ M) do not allow the determination of the $Co^{III/II}$ reduction potential due to hydrogen evolution and consequent irreversibility of the couple, and a complete and fully reliable study is not possible.

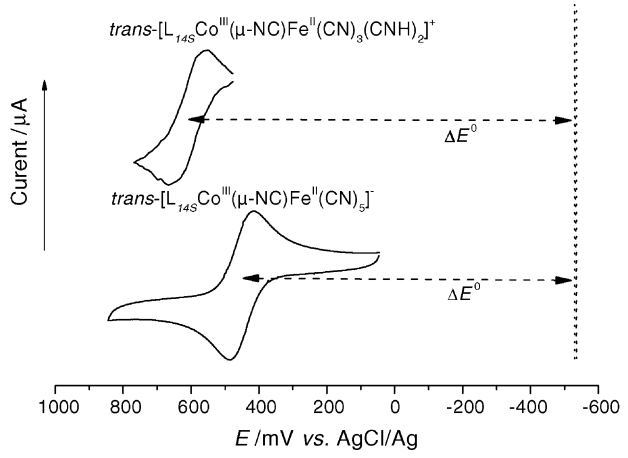

Fig. 7. $Fe^{III/II}$ cyclic voltammograms (platinum working electrode, 50 mV s^{-1}) of *trans*-$[L_{14S}Co^{III}(\mu\text{-NC})Fe^{II}(CN)_3(CNH)_2]^+$ (top) and *trans*-$[L_{14S}Co^{III}(\mu\text{-NC})Fe^{II}(CN)_5]^-$ (bottom). The vertical line corresponds to the reduction potential of the $Co^{III/II}$ couple in the deprotonated complex.

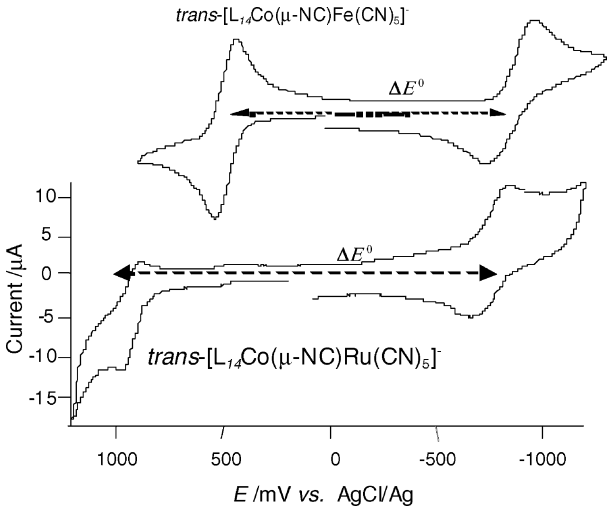

Fig. 8. Cyclic voltammograms (glassy carbon working electrode, 100 mV s^{-1}) of *trans*-$[L_{14}Co^{III}(\mu\text{-NC})Fe^{II}(CN)_5]^-$ (top) and *trans*-$[L_{14}Co^{III}(\mu\text{-NC})Ru^{II}(CN)_5]^-$ (bottom).

A further possibility that we have explored is the substitution of the donor metal ion (Fe^{II}) with its second row analogue Ru^{II}. In keeping with the redox potentials of $[Fe(CN)_6]^{3-/4}$ and $[Ru(CN)_6]^{3-/4-}$, the $Ru^{III/II}$ potential of *trans*-$[L_{14}Co^{III}(\mu\text{-NC})Ru^{II}(CN)_5]^-$ appears at 1150 mV (versus NHE), ca. 600 mV more positive than the corresponding $Fe^{III/II}$ wave of the iron analogue (Fig. 8). Indeed this couple is just within the potential window of the experiment (neutral aqueous solution, glassy carbon electrode), so, unlike the iron chemistry, the oxidized trivalent ruthenium complex is highly unstable and rapidly oxidizes water in returning to its Co^{III}/Ru^{II} form. By contrast, all of the oxidized Co^{III}–Fe^{III} analogues of the compounds in Table 2 are relatively stable at neutral pH, which has allowed their isolation and structural characterisation [65,70].

The deconvoluted electronic spectrum of this Co^{III}–Ru^{II} complex contains an MMCT band at 26300 cm^{-1} (E_{op}), which together with a calculated (from the difference between redox potentials) ΔG° value of 13600 cm^{-1}, produces a value of 12700 cm^{-1} for the reorganization energy (λ) according to Eq. (3). These values are in line with the data collected in Table 2 and the above-mentioned changes observed in the $Fe^{III/II}$ redox potentials on nitrile protonation. That is, the results are indicative that the redox potential-driven changes in ΔG° are the dominant factor in the observed differences for the values of the MMCT band maxima.

The introduction of other donors on the Fe^{II} moiety of the complex is currently being pursued. The use of the $[Fe(bipy)(CN)_4]^{2-}$ complex [71] has produced the mixed-valence complex $[L_{15}Co^{III}(\mu\text{-NC})Fe^{II}(bipy)(CN)_3]^+$, and important changes in both the position of the MMCT band and in the redox potentials are evident [72].

4. Redox processes

Evidently, the redox reactions involved in the preparative strategy of trinuclear complexes indicated above are very important, and these are related to "external" processes concerning the cobalt and iron centers separately. These reactions become more important as the changes in the MMCT band represent useful differences in the visible region of the electronic spectrum. In this respect, the appearance–disappearance of these bands when the outer-sphere oxidation of the mixed-valence compounds is carried out, leading to the oxidized Co^{III}–Fe^{III} complexes, is especially important for their possible applications [73].

4.1. Fe^{II} oxidation

The outer-sphere oxidation of mixed valence compounds has been studied on many occasions with complexes involving ruthenium. Standard $S_2O_8^{2-}$ oxidation of the complexes has been performed, and its outer-sphere character has been established [74–76]. We have studied a series of outer-sphere oxidation reactions on our dinuclear compounds at varying temperatures and pressures. The results obtained are collected in Table 4. In the same table, the values corresponding to the oxidation processes on the diprotonated derivatives, $[L_nCo^{III}(\mu\text{-NC})Fe^{II}(CN)_3(CNH)_2]^+$, are also collected [66,70]. These studies have allowed the comparison of the full series of reactions with important changes taking place at the iron center as seen in Table 5 and indicated before [66].

The rate law applied to these systems corresponds to Eq. (5).

$$k_{obs} = k_{et}K_{OS}[S_2O_8^{2-}] \quad (5)$$

The derived kinetic and activation parameters correspond to the second order rate constant $k_{et}K_{OS}$. Fortunately, the differences in K_{OS} are expected to be minimal for the series of complexes having the same degree of protonation (and charge) and the comparison can be directly related to differences in k_{et}.

It is clear that the entropy values are much more positive for the $[L_nCo^{III}(\mu\text{-NC})Fe^{II}(CN)_3(CNH)_2]^+$ complexes. This fact indicates that electrostriction at the iron center is very dominant and that a change in charge form $\{+1\};\{-2\}$ in the outer-sphere precursor species ($[L_nCo^{III}(\mu\text{-NC})Fe^{II}(CN)_3(CNH)_2]^+;S_2O_8^{2-}$) to $\{-1\};\{-2\}$ for the non-protonated form ($[L_nCo^{III}(\mu\text{-NC})Fe^{II}(CN)_5]^-;S_2O_8^{2-}$) is important in the liberation of solvent molecules from the respective solvation spheres. The difference is, nevertheless, compensated by much larger activation enthalpies for the reaction of the compound having two of the cyano groups protonated at their terminal N-atoms. This compensation is evident from the values determined for the rate constants that are very similar for the doubly-protonated and deprotonated systems, except for *trans*-$[L_{14S}Co^{III}(\mu\text{-NC})Fe^{II}(CN)_5]^-$ where important dif-

Table 4
Values of the kinetic and thermal and pressure activation parameters determined for the outer-sphere oxidation of the mixed-valence dinuclear complexes indicated, and their diprotonated forms, with $S_2O_8^{2-}$

Species	$k^{298} \times 10^2$ ($M^{-1}\,s^{-1}$)	$\Delta H^{\neq}$ ($kJ\,mol^{-1}$)	$\Delta S^{\neq}$ ($J\,K^{-1}\,mol^{-1}$)	$\Delta V^{\neq}$ ($cm^3\,mol^{-1}$)
cis-$[L_{13}Co^{III}(\mu\text{-NC})Fe^{II}(CN)_5]^-$	6.24	63 ± 3	−58 ± 10	19.6 ± 2.0
cis-$[L_{14}Co^{III}(\mu\text{-NC})Fe^{II}(CN)_5]^-$	6.80	58 ± 6	−72 ± 20	19.7 ± 0.6
trans-$[L_{14}Co^{III}(\mu\text{-NC})Fe^{II}(CN)_5]^-$	4.95	61 ± 1	−65 ± 3	4.1 ± 0.1
trans-$[L_{14S}Co^{III}(\mu\text{-NC})Fe^{II}(CN)_5]^-$	7.40	73 ± 2	−23 ± 6	8.1 ± 0.5
trans-$[L_{15}Co^{III}(\mu\text{-NC})Fe^{II}(CN)_5]^-$	16.2	55 ± 5	−76 ± 16	19.1 ± 1.7
cis-$[L_{13}Co^{III}(\mu\text{-NC})Fe^{II}(CN)_3(CNH)_2]^+$	6.98	114 ± 9	114 ± 29	12.7 ± 0.8
cis-$[L_{14}Co^{III}(\mu\text{-NC})Fe^{II}(CN)_3(CNH)_2]^+$	7.40	109 ± 7	98 ± 22	10.6 ± 1.2
trans-$[L_{14}Co^{III}(\mu\text{-NC})Fe^{II}(CN)_3(CNH)_2]^+$	5.61	80 ± 2	2 ± 7	1.5 ± 0.1
trans-$[L_{14S}Co^{III}(\mu\text{-NC})Fe^{II}(CN)_3(CNH)_2]^+$	18.0	91 ± 2	44 ± 7	Not determined
trans-$[L_{15}Co^{III}(\mu\text{-NC})Fe^{II}(CN)_3(CNH)_2]^+$	17.6	85 ± 4	23 ± 15	11.4 ± 0.7

ferences exist. Taking into account that for the doubly-protonated *trans*-systems depicted in Table 4, both enthalpies and entropies are lower and indicative of an important degree of hydrogen bonding in these very symmetrical arrangements [57,58], the difference for the L_{14S} systems is in accordance with the lack of two secondary amine protons in the Co^{III}-bound macrocycle.

Activation volumes are positive in all cases, although the values determined for the unprotonated forms, $[L_nCo^{III}(\mu\text{-NC})Fe^{II}(CN)_5]^-$, are larger. The expansion is not in agreement with electrostriction being solely involved in the precursor complex mentioned above; the values in that case would be expected to be definitively negative as the entropies are. These opposite trends between entropies and volumes of activation are related to the existence of solvent-assisted hydrogen bonding interactions [54,77–79]. For the doubly-protonated complexes such interactions are expected to be less, given the absence of two free terminal nitrogens in the coordination sphere of the iron center and the overall increase of positive charge. Consequently, the trends are in parallel. For the unprotonated complexes, the ordering derived from the values of the activation entropy includes an important degree of hydrogen bonding interactions that produce a very important increase in volume, even when electrostriction would imply the contrary. In this respect, the lower values found for the L_{14} and L_{14S} systems agree with a unique geometric distribution of the molecule that involves the two secondary amine protons 'lost' from the L_{14S} derivative, producing in this case values of $\Delta V^{\neq}$ closer to the expected from the trend in the other L_n complexes.

Table 5
Electrochemical $Fe^{III/II}$ redox data for the dinuclear complexes studied, protonated species in 1.0 M $HClO_4$, non-protonated in 1.0 M aqueous solution of $LiClO_4$

Species	E°_{red} ($Fe^{III/II}$) (mV)
cis-$[L_{13}Co^{III}(\mu\text{-NC})Fe^{II}(CN)_5]^-$	630
cis-$[L_{13}Co^{III}(\mu\text{-NC})Fe^{II}(CN)_3(CNH)_2]^+$	780
cis-$[L_{14}Co^{III}(\mu\text{-NC})Fe^{II}(CN)_5]^-$	600
cis-$[L_{14}Co^{III}(\mu\text{-NC})Fe^{II}(CN)_3(CNH)_2]^+$	780
trans-$[L_{14}Co^{III}(\mu\text{-NC})Fe^{II}(CN)_5]^-$	630
trans-$[L_{14}Co^{III}(\mu\text{-NC})Fe^{II}(CN)_3(CNH)_2]^+$	780
trans-$[L_{14S}Co^{III}(\mu\text{-NC})Fe^{II}(CN)_5]^-$	640
trans-$[L_{14S}Co^{III}(\mu\text{-NC})Fe^{II}(CN)_3(CNH)_2]^+$	800
trans-$[L_{15}Co^{III}(\mu\text{-NC})Fe^{II}(CN)_5]^-$	600
trans-$[L_{15}Co^{III}(\mu\text{-NC})Fe^{II}(CN)_3(CNH)_2]^+$	770

Table 6 collects the values for the oxidation of the same deprotonated $[L_nCo^{III}(\mu\text{-NC})Fe^{II}(CN)_5]^-$ complexes with $[Co(ox)_3]^{3-}$. In this case, the important ability of the outer-sphere oxidant to promote tight ion pairs [80] enabled the determination of a limiting-kinetics rate law such as that in Eq. (6).

$$k_{obs} = \frac{k_{et}K_{OS}[[Co(ox)_3]^{3-}]}{1 + K_{OS}[[Co(ox)_3]^{3-}]} \quad (6)$$

This rate law allows the separate determination of k_{et} and K_{OS} [61]. In this respect, the thermal and pressure activation parameters correspond to the real electron transfer process, the value of K_{OS} being in all cases in the 50–200 M^{-1} range for all the systems studied. The electron transfer process is again characterized by negative values of activation entropies and positive activation volumes. This is in the line with a solvent-assisted interaction as mentioned above. Unfortunately, the instability of the trisoxalatocobaltate(II) ion in acidic medium does not allow for comparison with the doubly-protonated species. Clearly, the value of $\Delta S^{\neq}$ for the L_{14S} complex is less negative than for the $S_2O_8^{2-}$ oxidation. The absence of two secondary amine hydrogen bonding donors is consistent with this.

4.2. Fe^{III} reduction

Isolation of the oxidized forms of our dinuclear complexes, devoid of MMCT bands, has enabled the study of reduction processes that regenerate the mixed-valence precursors. These Co^{III}–Fe^{III} compounds can be easily prepared by peroxodisulfate oxidation of the Co^{III}–Fe^{II} complexes [64]. The neutral charge of the oxidized complexes of formula $[L_nCo^{III}(\mu\text{-NC})Fe^{III}(CN)_5]$ leads to a much lower aqueous solubility than their monoanionic precursors and their isolation from dilute neutral solutions is straightforward. In dilute basic solution (pH 9.5–10), the oxidized complexes are reduced to the mixed-valence $[L_nCo^{III}(\mu\text{-NC})Fe^{II}(CN)_5]^-$ analogs and hydrogen peroxide has been identified as the

Table 6
Values of the kinetic and thermal and pressure activation parameters determined for the outer-sphere oxidation of the mixed-valence dinuclear complexes indicated with $[Co(ox)_3]^{3-}$

Species	k^{298} ($M^{-1}\,s^{-1}$)[a]	$\Delta H^{\ddagger}$ ($kJ\,mol^{-1}$)	$\Delta S^{\ddagger}$ ($JK^{-1}mol^{-1}$)	$\Delta V^{\ddagger}$ ($cm^3\,mol^{-1}$)
cis-$[L_{13}Co^{III}(\mu\text{-}NC)Fe^{II}(CN)_5]^-$	0.121	65 ± 3	-86 ± 10	14.6 ± 1.1
cis-$[L_{14}Co^{III}(\mu\text{-}NC)Fe^{II}(CN)_5]^-$	0.128	68 ± 5	-73 ± 17	16.9 ± 2.2
trans-$[L_{14}Co^{III}(\mu\text{-}NC)Fe^{II}(CN)_5]^-$	0.103	51 ± 2	-131 ± 8	11.5 ± 1.4
trans-$[L_{14S}Co^{III}(\mu\text{-}NC)Fe^{II}(CN)_5]^-$	0.0560	81 ± 6	-37 ± 19	13.0 ± 1.0
trans-$[L_{15}Co^{III}(\mu\text{-}NC)Fe^{II}(CN)_5]^-$	0.113	63 ± 6	-90 ± 19	17.9 ± 1.9

[a] K_{OS} in the 50–200 M^{-1} range for all the systems studied.

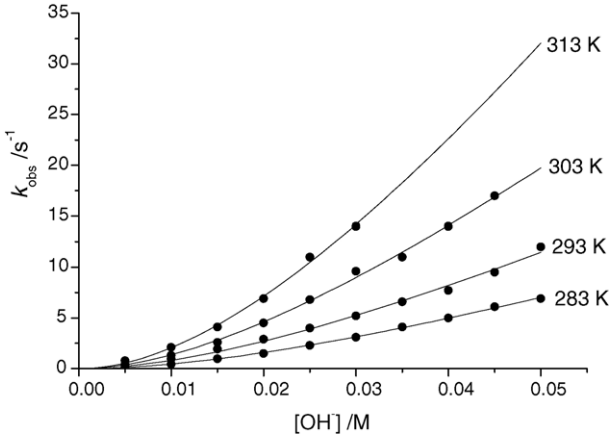

Fig. 9. Plot of k_{obs} vs. $[OH^-]$ for the reduction of *trans*-$[L_{14S}Co^{III}(\mu\text{-}NC)Fe^{III}(CN)_5]$ at different temperatures.

product of this process [70]. The reaction is very clean and fast, no oxygen is evolved in the absence of H_2O_2 decomposition, and the stoichiometry corresponds to the simple process $[L_nCo^{III}(\mu\text{-}NC)Fe^{III}(CN)_5] + OH^- \rightarrow [L_nCo^{III}(\mu\text{-}NC)Fe^{II}(CN)_5]^- + 1/2H_2O_2$. The reactions for all the dinuclear complexes derived from *cis*-L_{13}, *trans*-L_{14}, *trans*-L_{14S} and *trans*-L_{15} macrocycles at varying OH^- and Co^{III}–Fe^{III} complex concentrations, temperature and pressure have been studied. No dependence has been observed for the variation in the concentration of the complex, so we may disregard the involvement of reactions between two metal centers during or before the rate determining step, as observed for other water oxidizing systems [81,82]. Nevertheless, the $[OH^-]$ dependence of the observed rate constant is not simple, as seen in Fig. 9. The fitting of such dependence corresponds to a law of the type indicated by Eq. (7).

$$k_{obs} = \frac{a[OH^-]^2}{1 + b[OH^-]} \quad (7)$$

Only the term *a* shows any dependence on temperature and pressure, while the term *b* is constant for all systems in the 20–25 M^{-1} margin. A mechanism consistent with these observations is indicated in Scheme 6, where the term *b* corresponds to the constant depicted as K_{add}, while the ratio *a*/*b* corresponds to the second order rate constant $k_{et}K_{dep}$. The mechanism involves the formation of an OH^- adduct of the oxidized Co^{III}–Fe^{III} complex similar to that found for other $[Fe(CN)_6]^{3-}$ systems [83,84], with an equilibrium constant of ca. 20 M^{-1} for all compounds. Further deprotonation of this adduct with a second OH^- ion explains the second order dependence on its concentration. The O^{2-} adduct species formed reacts via an inner-sphere process to produce the final Co^{III}–Fe^{II} complex. The final hydrogen peroxide detected is produced via the fast dimerization and decomposition processes indicated in Scheme 6.

The values derived from the kinetic and thermal and pressure activation parameters are collected in Table 7. From these results it is clear that the enthalpic demands of the water to hydrogen peroxide oxidation by the Co^{III}–Fe^{III} complexes are very small while activation entropies are very negative and parallel the determined values for $\Delta V^{\ddagger}$. This agrees very

$$[L^nCo^{III}NCFe^{III}(CN)_5]^0 + OH^- \underset{}{\overset{K_{add}}{\rightleftharpoons}} \{[L^nCo^{III}NCFe^{III}(CN)_5]\cdot OH\}^-$$

$$\{[L^nCo^{III}NCFe^{III}(CN)_5]\cdot OH\}^- + OH^- \overset{K_{dep}}{\rightleftharpoons} \{[L^nCo^{III}NCFe^{III}(CN)_5]\cdot O\}^{2-} + H_2O$$

$$\{[L^nCo^{III}NCFe^{III}(CN)_5]\cdot O\}^{2-} \xrightarrow{k_{et}} \{[L^nCo^{III}NCFe^{II}(CN)_5]\cdot O^{\cdot}\}^{2-}$$

$$\{[L^nCo^{III}NCFe^{II}(CN)_5]\cdot O^{\cdot}\}^{2-} \xrightarrow{fast} 1/2\ \{[L^nCo^{III}NCFe^{II}(CN)_5]\cdot O\}_2^{4-}$$

$$1/2\ \{[L^nCo^{III}NCFe^{II}(CN)_5]\cdot O\}_2^{4-} \xrightarrow{fast} [L^nCo^{III}NCFe^{II}(CN)_5]^- + 1/2\ O_2^{2-}$$

$$1/2\ O_2^{2-} + H_2O \overset{K_a'^{-1}}{\rightleftharpoons} 1/2\ O_2H^- + OH^-$$

Scheme 6.

Table 7
Kinetic and thermal and pressure activation parameters for the water oxidation processes by the complexes $[L_nCo^{III}NCFe^{III}(CN)_5]$ studied ($I = 1.0$ M $LiClO_4$)

Complex	K_{add} (M^{-1})[a]	$k_{et}{}^{298}K_{dep} \times 10^3$ ($M^{-1}\,s^{-1}$)	$\Delta H^{\neq}$ (kJ mol^{-1})	$\Delta S^{\neq}$ (J K^{-1} mol^{-1})	$\Delta V^{\neq}$ (cm^3 mol^{-1})
cis-$[L_{13}Co^{III}NCFe^{III}(CN)_5]$	21	2.2	27 ± 1	-91 ± 5	Not determined
trans-$[L_{14}Co^{III}NCFe^{III}(CN)_5]$	22	0.20	28 ± 1	-108 ± 4	-8.9 ± 0.5
trans-$[L_{14S}Co^{III}NCFe^{III}(CN)_5]$	22	0.60	35 ± 3	-76 ± 9	-5.5 ± 0.4
trans-$[L_{15}Co^{III}NCFe^{III}(CN)_5]$	26	24	15 ± 1	-113 ± 5	-9.6 ± 0.3

[a] Average for the reaction conditions studied.

well with the inner-sphere character of the process depicted in Scheme 6, no hydrogen bonding interactions are expected, and a good correlation between $\Delta S^{\neq}$ and $\Delta V^{\neq}$ must exist. The enthalpy demands are also expected to be very low and they do not have to correlate with the redox potentials of the iron center, as observed when Tables 6 and 7 are compared.

In this respect, it is interesting to note that the reaction mechanism proposed also explains the formation of the mixed-valence complex $[L_nCo^{III}(\mu\text{-NC})Fe^{II}(CN)_5]^-$ in the base-assisted substitution process of water by $[Fe^{III}(CN)_6]^{3-}$ in $[Co^{III}L_n(H_2O)]^{3+}$ as indicated in Section 2.

4.3. Co^{III} reduction

The formation of dinuclear Co^{II}–Fe^{II} complexes is not as straightforward as seen in analogous ruthenium(III)/iron(II) systems, where the existence of four oxidation states has been claimed in order to explain the redox reactivity of the complexes [74]. With our compounds, the preparation of Co^{II}–Fe^{II} derivatives can only be achieved transiently due to the air sensitivity and lability of the reduced compounds.

Although the transient formation of these complexes is clear from cyclic voltammetry experiments, their extreme substitutional lability makes isolation problematic. However, the role of these reduced compounds in the formation of trinuclear mixed-valence complexes (Scheme 4) appears to be crucial [54,63]. Pulse radiolysis experiments have been carried out on *trans*-$[L_{14}Co^{III}(\mu\text{-NC})Fe^{II}(CN)_5]^-$ and *cis*-$[L_{14}Co^{III}(\mu\text{-NC})Fe^{II}(CN)_5]^-$, *trans*-$[L_{14}Co^{III}(\mu\text{-NC})Ru^{II}(CN)_5]^-$ and *trans*-$[L_{14S}Co^{III}(\mu\text{-NC})Fe^{II}(CN)_5]^-$

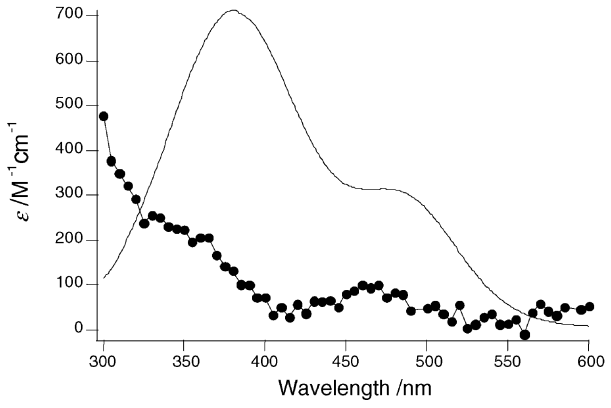

Fig. 10. UV–vis spectrum of *trans*-$[L_{14}Co^{III}(\mu\text{-NC})Ru^{II}(CN)_5]^-$ (solid line) and the product of a one electron reduction by pulse radiolysis to produce *trans*-$[L_{14}Co^{II}(\mu\text{-NC})Ru^{II}(CN)_5]^{2-}$ (closed circles).

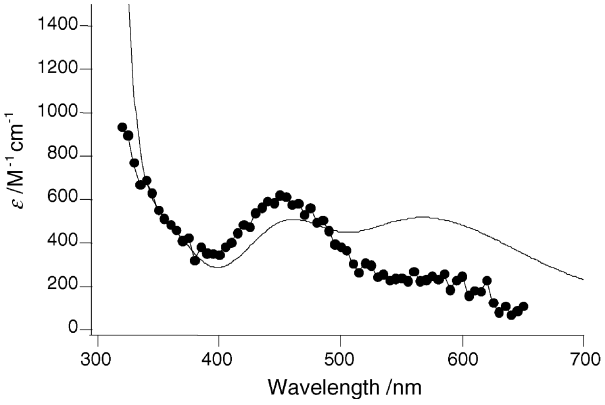

Fig. 11. UV–vis spectrum of the complex *trans*-$[L_{14S}Co^{III}(\mu\text{-NC})Fe^{II}(CN)_5]^-$ (solid line) upon one electron reduction by pulse radiolysis to produce *trans*-$[L_{14S}Co^{II}(\mu\text{-NC})Fe^{II}(CN)_5]^{2-}$ (closed circles).

where the reductant was the aquated electron [64,65,67]. In all cases, disappearance of the MMCT band is complete upon reduction (Figs. 10 and 11). Nevertheless, the characteristics of the spectra are not the same in each case. While the visible spectra of the reduced *trans*-$[L_{14}Co^{II}(\mu\text{-NC})Fe^{II}(CN)_5]^{2-}$ and *cis*-$[L_{14}Co^{II}(\mu\text{-NC})Fe^{II}(CN)_5]^{2-}$ and *trans*-$[L_{14}Co^{II}(\mu\text{-NC})Ru^{II}(CN)_5]^-$ complexes are essentially featureless, and indicative of a high-spin d^7 Co^{II} complex, the spectrum of sulfur analogue *trans*-$[L_{14S}Co^{II}(\mu\text{-NC})Fe^{II}(CN)_5]^{2-}$ retains a prominent absorption band around 450 nm consistent with a low-spin d^7 electronic ground state [85,86]. This is in agreement with well characterized low-spin Co^{II} complexes in mixed donor (N,S) coordination environments [87,88]. Further studies with softer ligand systems are currently under way with the $L_{15\Phi S}$ macrocycle (Scheme 3) in order to stabilize the Co^{II}–Fe^{II} as much as possible and so open up more possibilities for the study of these complexes.

5. Conclusions

In this review, different variables affecting the spectroscopic (MMCT bands), electrochemical (redox potentials) and chemical redox properties of a series of dinuclear mixed-valence cyano-bridged $[L_nCo^{III}(\mu\text{-NC})Fe^{II}(CN)_5]^-$ compounds have been reviewed.

The simple change of the macrocyclic ring size of the compounds (n in L_n) only produces minor effects both on the redox potentials of the Co^{III} acceptor center and the MMCT band. Nevertheless, changes from *cis* to *trans* config-

uration in the macrocyclic ring (Scheme 3) produce important changes in the redox potential of the same center. A larger reorganization energy (λ) for the *cis* isomer compensates for this difference, and little net effect on the MMCT transition energy is observed. Important changes in the energy of the MMCT band appear when changes to the macrocyclic donor atoms are introduced, i.e., pentaamine L_{14} to aminothioether L_{14S}. Changes in the electron donor unit $\{Fe^{II}(CN)_5\}$ of the complex, such as nitrile protonation and/or substitution of iron by ruthenium, also produce large changes in E_{op}. Application of Hush theory indicates that the free energy difference between the redox isomers is the dominant effect in the variation of the MMCT energy in these systems.

The outer-sphere redox processes of these complexes have also been studied. Oxidation of the iron center of these Co^{III}–Fe^{II} compounds results in the loss of the MMCT band, producing a marked change in their color from purple-maroon to yellow. Reduction of the electron acceptor Co^{III} centers also results in the disappearance of the MMCT band. The outer-sphere oxidation of the $\{Fe^{II}(CN)_5\}$ moiety by $S_2O_8^{2-}$ and $[Co(ox)_3]^{3-}$ has been studied from a kinetico-mechanistic perspective proving that the process is dominated by important solvent-assisted interactions between redox pairs.

The oxidized forms of the complexes, $[L_nCo^{III}(\mu\text{-}NC)Fe^{III}(CN)_5]$, have been shown to oxidize water stochiometrically to H_2O_2 in alkaline medium. The process has been studied mechanistically, and found to proceed via an OH^- adduct intermediate that undergoes an inner-sphere redox reaction. The mixed-valence Co^{III}–Fe^{II} form of the dinuclear compounds is the final complex of the redox process.

A mechanistically designed strategy has been employed for the preparation of almost all the systems reported. The process takes advantage of the outer-sphere redox reactions occurring between $[CoL_n(H_2O)]^{3+}$ and $[Fe(CN)_6]^{4-}$ that renders substitutionally labile Co^{II} complexes and $[Fe(CN)_6]^{3-}$. The substitution of water on inert $[CoL_n(H_2O)]^{3+}$ by $[Fe(CN)_6]^{3-}$ is the only possibility for a simple reaction producing a dinuclear species. The reactions are very slow, but they can be accelerated in alkaline medium via known base-catalysed substitution mechanisms. By doing so, the final compounds obtained, via the abovementioned water oxidation process, are $[L_nCo^{III}(\mu\text{-}NC)Fe^{II}(CN)_5]^-$. The knowledge of the reaction mechanisms operating on these simple systems has allowed the design of clean preparative routes to these interesting complexes.

Acknowledgements

We would like to thank the Australian Research Council and the Ministerio de Ciencia y Tecnología for financial support.

References

[1] H. Vahrenkamp, A. Geiss, G.N. Richardson, J. Chem. Soc. Dalton Trans. (1997) 3643.
[2] W.M. Laidler, R.G. Denning, T. Verbiest, E. Chauchard, A. Persoons, Nature 363 (1993) 58.
[3] M.B. Robin, P. Day, Adv. Inorg. Chem. Radiochem. 10 (1967) 247.
[4] N.S. Hush, Prog. Inorg. Chem. 8 (1967) 391.
[5] C. Creutz, Prog. Inorg. Chem. 30 (1983) 1.
[6] G.C. Allen, N.S. Hush, Prog. Inorg. Chem. 8 (1967) 357.
[7] R.A. Marcus, N. Sutin, Biochim. Biophys. Acta 811 (1985) 265.
[8] M.B. Robin, P. Day, Adv. Inorg. Chem. Radiochem. 10 (1967) 247.
[9] R.A. Marcus, Angew. Chem. Int. Ed. 32 (1993) 1111.
[10] J.T. Hupp, G.A. Neyhart, T.J. Meyer, E.M. Kober, J. Phys. Chem. 96 (1992) 10820.
[11] P. Chen, T. Meyer, J. Chem. Rev. 98 (1998) 1439.
[12] V. Gutmann, The Donor–Acceptor Approach to Molecular Interactions, Plenum Press, New York, 1978.
[13] F. Sánchez, P. Pérez-Tejeda, M. López-López, Inorg. Chem. 38 (1999) 1780.
[14] S.F. Nelsen, R.F. Ismagilov, D.R. Powell, J. Am. Chem. Soc. 119 (1997) 10213.
[15] G. López-Pérez, R. Prado-Gotor, F. Sánchez, M. López-López, D. González-Arjona, P. Pérez-Tejeda, F. Bozoglián, G. González, M. Martínez, submitted for publication.
[16] R.A. Marcus, J. Phys. Chem. B 102 (1998) 10071.
[17] S.B. Piepho, E.R. Krausz, P.N. Schatz, J. Am. Chem. Soc. 100 (1978) 2996.
[18] P.S. Braterman, J. Chem. Soc. A 10 (1966) 1471.
[19] M.B. Robin, Inorg. Chem. 1 (1962) 337.
[20] E.M. Kober, K.A. Goldsby, D.N.S. Narayana, T.J. Meyer, J. Am. Chem. Soc. 105 (1983) 4303.
[21] J.T. Hupp, T. Meyer, J. Inorg. Chem. 26 (1987) 2332.
[22] J.R. Schoonover, C.J. Timpson, T.J. Meyer, C.A. Bignozzi, Inorg. Chem. 31 (1992) 3185.
[23] A. Haim, W.K. Wilmarth, J. Am. Chem. Soc. 83 (1961) 509.
[24] A. Vogler, H. Kunkely, Ber. Bunsen-Ges. Phys. Chem. 79 (1975) 301.
[25] R.A. De Castello, C.P. Mac-Coll, N.B. Egen, A. Haim, Inorg. Chem. 8 (1969) 699.
[26] R.A. De Castello, C. Piriz Mac-Coll, A. Haim, Inorg. Chem. 10 (1971) 203.
[27] A. Burewicz, A. Haim, Inorg. Chem. 27 (1988) 1611.
[28] A. Vogler, H. Kunkely, Ber. Bunsen-Ges. Phys. Chem. 79 (1975) 83.
[29] A. Vogler, A.H. Osman, H. Kunkely, Coord. Chem. Rev. 64 (1985) 159.
[30] A. Vogler, A.H. Osman, H. Kunkely, Inorg. Chem. 26 (1987) 2337.
[31] P. Forlano, L.M. Baraldo, J.A. Olabe, C.O. Della Vedova, Inorg. Chim. Acta 223 (1994) 37.
[32] A. Vogler, J. Kisslinger, J. Am. Chem. Soc. 104 (1982) 2311.
[33] R. Glauser, U. Hauser, F. Herren, A. Ludi, P. Roder, E. Schmidt, H. Siegenthaler, F. Wenk, J. Am. Chem. Soc. 95 (1973) 8457.
[34] D. Chatterjee, H.C. Bajaj, A. Das, Inorg. Chem. 32 (1993) 4049.
[35] P. Forlano, F.D. Cukiernik, O. Poizat, J.A. Olabe, J. Chem. Soc. Dalton Trans. (1997) 1595.
[36] G. Stochel, Polyhedron 13 (1994) 155.
[37] G. Emschwiller, C. Friedrich, Acad. Sci. Ser. IIc: Chim. 278 (1974) 1335.
[38] B.W. Pfennig, J.V. Lockard, J.L. Cohen, D.F. Watson, D.M. Ho, A.B. Bocarsly, Inorg. Chem. 38 (1999) 2941.
[39] A.W. Adamson, E. Gonick, Inorg. Chem. 2 (1963) 129.
[40] D.H. Huchital, R.G. Wilkins, Inorg. Chem. 6 (1967) 1022.
[41] F. Scandola, R. Argazzi, C.A. Bignozzi, C. Chiorboli, M.T. Indelli, M.A. Rampi, Coord. Chem. Rev. 125 (1993) 283.
[42] C. Creutz, H. Taube, J. Am. Chem. Soc. 91 (1969) 3988.
[43] A.G. Sharpe, The Chemistry of Cyano Complexes of the Transition Metals, Academic Press, London, 1976.

[44] A.B.P. Lever, Inorganic Electronic Spectroscopy, second ed., Elsevier, Amsterdam, 1984.
[45] H. Kunkely, A. Vogler, Inorg. Chim. Acta 209 (1993) 93.
[46] H. Kunkely, V. Pawlowski, A. Vogler, Inorg. Chim. Acta 225 (1994) 327.
[47] D. Chatterjee, Polyhedron 18 (1999) 1767.
[48] Y.H. Dong, J.T. Hupp, Inorg. Chem. 31 (1992) 3322.
[49] D.H. Huchital, R.G. Wilkins, Inorg. Chem 6 (1967) 1022.
[50] M. Zhou, B.W. Pfennig, J. Steiger, D. Van Engen, A.B. Bocarsly, Inorg. Chem. 29 (1990) 2456.
[51] C.C. Chang, B. Pfennig, A.B. Bocarsly, Coord. Chem. Rev. 208 (2000) 33.
[52] P. Comba, A.F. Sickmuller, Inorg. Chem. 36 (1997) 4500.
[53] M. Martínez, M.A. Pitarque, J. Chem. Soc. Dalton Trans. (1995) 4107.
[54] M. Martínez, M. Pitarque, R. van Eldik, Inorg. Chim. Acta 256 (1997) 51.
[55] D.H. Huchital, R.J. Hodges, Inorg. Chem. 12 (1973) 998.
[56] L. Rosenhein, D. Speiser, A. Haim, Inorg. Chem. 13 (1974) 1571.
[57] G. González, M. Martínez, E. Rodríguez, Eur. J. Inorg. Chem. (2000) 1333.
[58] F. Benzo, P.V. Bernhardt, G. González, M. Martínez, J. Chem. Soc. Dalton Trans. (1999) 3973.
[59] F. Bozoglián, G. González, M. Martínez, M. Queirolo, B. Sienra, Inorg. Chim. Acta 318 (2001) 191.
[60] M.L. Tobe, J. Burgess, Inorganic Reaction Mechanisms, Addison Wesley Longman, Harlow, 1999.
[61] R.G. Wilkins, Kinetics and Mechanisms of Reactions of Transition Metal Complexes, second ed., VCH, Weinheim, 1991.
[62] T.W. Hambley, G.A. Lawrance, M. Martínez, B.W. Skelton, A.L. White, J. Chem. Soc. Dalton Trans. (1992) 1643.
[63] P.V. Bernhardt, M. Martínez, Inorg. Chem. 38 (1999) 424.
[64] P.V. Bernhardt, B.P. Macpherson, M. Martínez, Inorg. Chem. 39 (2000) 5203.
[65] P.V. Bernhardt, B.P. Macpherson, M. Martínez, J. Chem. Soc. Dalton Trans. (2002) 1435.
[66] P.V. Bernhardt, F. Bozoglián, B.P. Macpherson, M. Martínez, G. González, B. Sienra, Eur. J. Inorg. Chem. (2003) 2512.
[67] P.V. Bernhardt, F. Bozoglián, B.P. Macpherson, M. Martínez, Dalton Trans. (2004) 2582.
[68] P.V. Bernhardt, F. Bozoglián, B.P. Macpherson, M. Martínez, C. del Rio, unpublished results, 2004.
[69] T.W. Hambley, Inorg. Chem. 27 (1988) 2496.
[70] P.V. Bernhardt, F. Bozoglián, B.P. Macpherson, M. Martínez, A.E. Merbach, G. González, B. Sienra, Inorg. Chem. 43 (2004) 7185.
[71] A. Schilt, J. Am. Chem. Soc. 82 (1960) 3000.
[72] P.V. Bernhardt, F. Bozoglián, M. Font-Bardía, B.P. Macpherson, M. Martínez, X. Solans, unpublished results, 2004.
[73] D.R. Rosseinsky, R. Mortimer, J. Adv. Mater. 13 (2001) 783.
[74] A.E. Almaraz, L.A. Gentil, L.M. Baraldo, J.A. Olabe, Inorg. Chem. 35 (1996) 7718.
[75] F. Fagalde, N.E. Katz, V.G. Povse, J.A. Olabe, Polyhedron 18 (1998) 25.
[76] A.R. Parise, L.M. Baraldo, J.A. Olabe, Inorg. Chem. 35 (1996) 5080.
[77] P.V. Bernhardt, C. Gallego, M. Martínez, T. Parella, Inorg. Chem. 41 (2002) 1747.
[78] C. Gallego, G. González, M. Martínez, A.E. Merbach, Organometallics 23 (2004) 2434.
[79] M. Martínez, M. Pitarque, R. van Eldik, J. Chem. Soc. Dalton Trans. (1994) 3159.
[80] R.M.L. Warren, A.G. Lappin, A. Tatehata, Inorg. Chem. 31 (1992) 1566.
[81] M. Anbar, I. Pecht, J. Am. Chem. Soc. 89 (1967) 2553.
[82] A.L. Feig, M. Becker, S. Schindler, R. van Eldik, S. Lippard, J. Inorg. Chem. 35 (1996) 2590.
[83] J.M. Lancanster, R.S. Murray, J. Chem. Soc. A (1971) 2755.
[84] R.S. Murray, J. Chem. Soc. Dalton Trans. (1974) 2381.
[85] P.V. Bernhardt, L.A. Jones, Inorg. Chem. 38 (1999) 5086.
[86] T.M. Donlevy, L.R. Gahan, T.W. Hambley, R. Stranger, Inorg. Chem. 31 (1992) 4376.
[87] T.M. Donlevy, L.R. Gahan, T.W. Hambley, Inorg. Chem. 33 (1994) 2668.
[88] R.V. Dubs, L.R. Gahan, A.M. Sargeson, Inorg. Chem. 22 (1983) 2523.